Applied Physics Letters

Spatially and momentum resolved energy electron loss spectra from an ultra-thin $PrNiO_3$ layer

Cite as: Appl. Phys. Lett. **106**, 203102 (2015); https://doi.org/10.1063/1.4921405
Submitted: 23 January 2015 . Accepted: 09 May 2015 . Published Online: 18 May 2015

M. K. Kinyanjui, G. Benner, G. Pavia, F. Boucher, H.-U. Habermeier, B. Keimer, and U. Kaiser

Spatially and momentum resolved energy electron loss spectra from an ultra-thin $PrNiO_3$ layer

M. K. Kinyanjui,[1,a)] G. Benner,[2] G. Pavia,[2] F. Boucher,[3] H.-U. Habermeier,[4] B. Keimer,[4] and U. Kaiser[1]

[1]*Central Facility of Electron Microscopy, University of Ulm, Albert-Einstein Allee 11, 89081 Ulm, Germany*
[2]*Carl Zeiss Microscopy GmbH, Carl-Zeiss-Str. 22, 73447 Oberkochen, Germany*
[3]*Institut des Matériaux Jean Rouxel, UMR6502, CNRS - Université de Nantes, 2 rue de la Houssinière, B.P.32229, 44322 Nantes Cedex, France*
[4]*Max Planck Institute for Solid State Research, Heisenbergstrasse 1, D-70579 Stuttgart, Germany*

(Received 23 January 2015; accepted 9 May 2015; published online 18 May 2015)

We present an experimental approach which allows for the acquisition of spectra from ultra-thin films at high spatial, momentum, and energy resolutions. Spatially and momentum (q) resolved electron energy loss spectra have been obtained from a 12 nm ultra-thin $PrNiO_3$ layer using a nano-beam electron diffraction based approach which enabled the acquisition of momentum resolved spectra from individual, differently oriented nano-domains and at different positions of the $PrNiO_3$ thin layer. The spatial and wavelength dependence of the spectral excitations are obtained and characterized after the analysis of the experimental spectra using calculated dielectric and energy loss functions. The presented approach makes a contribution towards obtaining momentum-resolved spectra from nanostructures, thin film, heterostructures, surfaces, and interfaces. © *2015 AIP Publishing LLC*.
[http://dx.doi.org/10.1063/1.4921405]

Increased interest in nanostructures, ultra-thin films, and heterostructures calls for experimental probes with high spatial resolution. Electron Energy Loss Spectroscopy (EELS) in the transmission electron microscope (TEM) is one method capable of probing electronic, magnetic, and atomic structure at high spatial resolution. In addition, it is possible to obtain momentum-resolved EELS spectra (MREELS) showing the momentum (q) dependence (dispersion) of various excitations thereby probing bandstructures, bonding anisotropy, as well as indirect, and dipole-forbidden excitations.[1–8] However, obtaining momentum resolved spectra from ultrathin films, heterostructures, and nanostructures at high spatial resolution has remained difficult.

The momentum information is accessed by acquiring the EELS spectra in the diffraction plane of the TEM.[3–17] The scattering geometry for a MREELS experiment is presented in Fig. 1(a). θ is the scattering angle and $\boldsymbol{q}$ is the scattering vector given by $\boldsymbol{k_0} - \boldsymbol{k'}$ with $\boldsymbol{k_0}$ and $\boldsymbol{k'}$ being the wave vectors of incident and inelastically scattered electrons, respectively.[1,2] Projected direction and magnitude of scattering angles are obtained in the electron diffraction pattern and are related to the direction and magnitude of $|\boldsymbol{q}|$ through $\boldsymbol{q}^2 = \boldsymbol{k}_0^2\,(\theta^2 + \theta_E)^{1/2}$, where θ_E is the characteristic angle. Selecting a set of Bragg diffraction spots with a slit (see Fig. 1(b)) allows electrons scattered at a certain scattering angle into the spectrometer giving a spectrum showing energy loss (ΔE) and momentum transfer ($|q|$).

The obtainable spatial resolution depends on the electron beam/spot size as dictated by the angle of convergence of the primary electron beam, lens aberrations, and the diameter of the selecting aperture.[1,9] MREELS spectra are mostly obtained with a parallel electron beam having low convergence and spatial resolution in the range 0.1–1.0 μm. Recently, Hage *et al*. presented an approach to obtain MREELS spectra using a highly converged electron beam.[18] However, due to overlapping discs, the acquisition of momentum information along a defined direction in the reciprocal space is difficult resulting in momentum resolution between 0.5 and 1.2 $Å^{-1}$. We present a nano-beam electron diffraction (NBED) approach used to obtain MREELS spectra from a 12 nm thick $PrNiO_3$ layer at high spatial resolution ~2 nm at the same time easily accessing momentum information since the diffraction pattern spots are not overlapping.[19] This is demonstrated in Fig. 1(b) where the schematic diffraction spots for parallel beam diffraction (1), converged beam diffraction (2), and NBED pattern (3) are compared.

Interest in thin films/heterostructures of $PrNiO_3$ and other rare-earth nickelates ($RNiO_3$, R = rare earth trivalent cation) is motivated by the fact that their properties can be

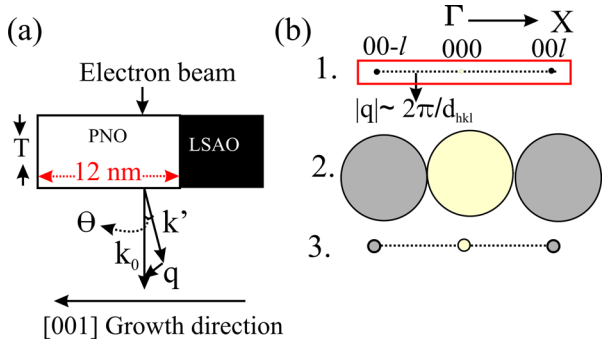

FIG. 1. (a) Scattering geometry for the MREELS experiment. T is TEM sample thickness in the direction of the beam. (b) Schematic showing the reciprocal space for parallel (1), converged (2), and nano-beam electron diffraction (3). The rectangle shows the position of the selecting slit placed parallel to the 00*l*, 00-*l* diffraction spots.

[a)]Author to whom correspondence should be addressed. Electronic mail: michael.kinyanjui@uni-ulm.de

modified by varying layer thickness, epitaxial strain, and layer confinement.[20,21] Bulk $PrNiO_3$ undergoes a metal-insulator transition at 120 K with structural changes from the room temperature orthorhombic (Pbnm) structure to monoclinic (P21/n) structure below the metal-insulator temperature.[21] The effects of layer thickness, microstructure, epitaxial strain, and confinement in heterostructure geometry on the properties of $PrNiO_3$ are still not understood. Spatially and momentum resolved spectroscopy may enable probing the effects of layer geometry/thickness, presence of interfaces and surfaces on the spectra. This method also allows for the dispersion of various excitations to be obtained. In addition, orbital excitations including dipole-forbidden excitations which are only observed $q \gg 0\,\text{Å}^{-1}$ can be obtained.[13] These excitations provide information regarding local bonding symmetry as well as possible changes in atomic/electronic structure accompanying temperature-induced phase transitions.[13,22]

We used pulsed laser deposition to grow 12 nm thick $PrNiO_3$ and 70 nm thick $LaNiO_3$ layers on a $LaSrAlO_4$ (001) substrate. TEM samples were then thinned using a focussed ion beam (FIB) to a TEM sample thickness (T) of 20–30 nm in the beam direction perpendicular to the growth direction. MREELS spectra were obtained using a Cs-corrected Libra TEM operating at 80 kV equipped with an energy monochromator and an in-column Omega energy filter. In the NBED mode, the obtained electron beam spot size was 2 nm and convergence angle of ~1 mrad.[19] In this configuration, momentum resolutions between 0.2 and $0.4\,\text{Å}^{-1}$ could be obtained.[24] Electronic structure and theoretical EELS spectra for $|\boldsymbol{q}| \rightarrow 0$ were calculated using the WIEN2k code.[23,24] Additional theoretical EELS spectra with the inclusion of local field effects were obtained using the VASP code.[24]

Figure 2(a) displays a Z-contrast image of the $PrNiO_3$ layer on $LaSrAlO_4$ substrate. NBED patterns obtained at 300 K and at various positions of the $PrNiO_3$ layer are presented in Figs. 2(b) and 2(c) showing the nano-domain nature of the $PrNiO_3$ film. Figures 2(b) and 2(c) display the NBED patterns from [010] and [110] oriented domains, respectively. The 000, −200, 200, as well as 002, 00–2 diffraction spots are marked with the circle, square, and triangle, respectively. To obtain a MREELS spectra from individual domains, a selecting slit is placed parallel to the 200, −200 and 002, 00–2 diffraction spots in the NBED patterns from the [010] and [110] oriented domains, respectively. This corresponds to spectra along $\boldsymbol{q}$ // [100] and $\boldsymbol{q}$ // [001].

A ω-q intensity map showing energy loss (vertical axis) as a function of momentum (horizontal axis) is displayed in Fig. 3(a). For a slit placed parallel to the 200 and 200 spots (i.e., $\boldsymbol{q}$ // [100]), the distance between the Brag spots is $2.31\,\text{Å}^{-1}$. By obtaining MREELS spectra along different directions in the BZ, the dependence of the excitations on the direction of $\boldsymbol{q}$ (spatial dependence) is thus determined. In addition, the dependence of the MREELS spectra with the magnitude of |q| along a particular direction in the BZ (wavelength dependence) can also be investigated. Figures 3(b) and 3(c) display individual EELS spectra obtained for various values along **q** // [100] from the domain variant [010] and along **q** // [001] from the domain variant [110], respectively. MREELS spectra are obtained within the range of $0 \leq |q| \leq 0.8\,\text{Å}^{-1}$.

In both cases, peak features are labeled A, B, C, D, E, and F at 1.3 eV, 7.0 eV, 13.0 eV, 18.0 eV, 24.0 eV, and 31.0 eV, respectively. Peak A shows a very weak dispersion, is very sharp at low momentum values and its intensity decreases with increasing momentum. Peaks C and F are on the other hand dispersive. In addition, spectra obtained along $\boldsymbol{q}$ // [001] show a splitting of peak F at high momentum transfer. The splitting is most possibly due to multiple-inelastic scattering involving the forbidden 0 0 1 type reflection observed in the NBED pattern from the [110] oriented domain. The origin of this reflection is still unclear but it is possible that it originates from double diffraction.[24] Despite the fact that multiple scattering is mostly undesirable, here it is proof that the MREELS spectra were obtained from two differently oriented nano-domains.

In the following discussion, we try to identify the nature and the origin of the observed peaks as well as effects of layer thickness on the experimental spectra. We determine the nature and the origin of various peaks by comparing the experimental EELS spectra (at $q \sim 0\,\text{Å}^{-1}$) with calculated EELS spectra and dielectric functions both with and without the inclusion of local field effects (LFE).[25–29] This is presented in Fig. 4(a) for energy loss spectra and in Fig. 4(b) for the dielectric constants. In Fig. 4(a), the calculated energy

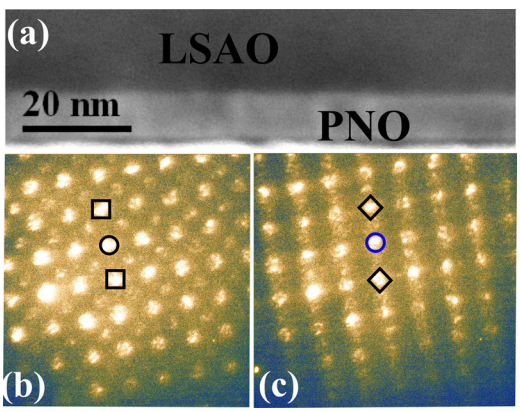

FIG. 2. (a) Z-contrast TEM image of a 12 nm thick $PrNiO_3$ layer (b) and (c) NBED patterns from (b) domain oriented in the [010] direction. (c) Domain oriented in the [110] direction. The 000, −200, and 00–2 diffraction spots are marked with a circle, square, and triangle, respectively.

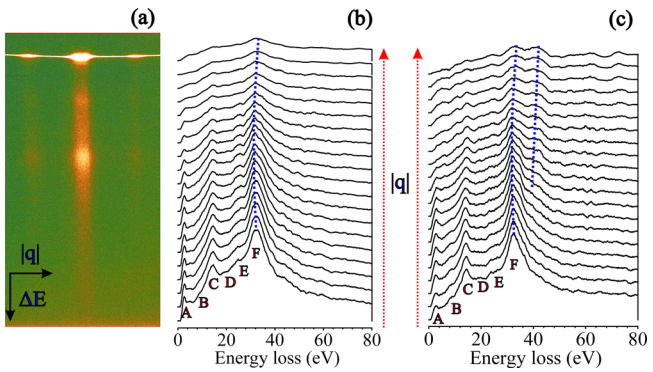

FIG. 3. (a) Representative intensity map (ω-|q| map) showing energy loss, ΔE (vertical axis) as a function of |q| (horizontal axis). (b) Individual EELS spectra at various values of **q** // [100] from the domain variant [010]. (c) **q** // [001] from the domain variant [110].

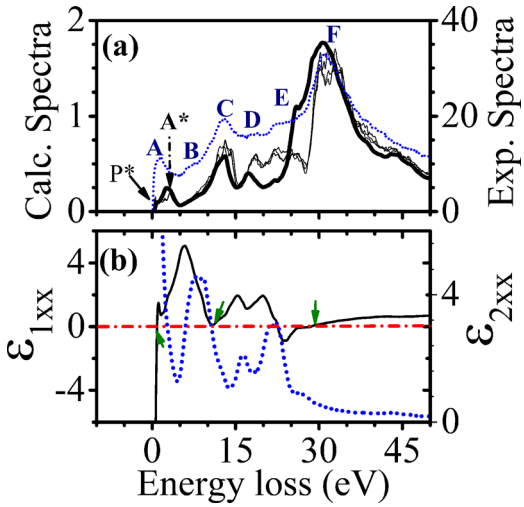

FIG. 4. (a) Experimental EELS spectra for $PrNiO_3$ at $|q| \sim 0\,Å^{-1}$ (dotted line) compared with calculated spectra without local field effects (thick line) and with inclusion of local field effects (thin lines). (b) Calculated ε_{2xx} (dashed line), calculated ε_{1xx} (solid line). The arrows mark where the ε_1 crosses the energy axis with a positive slope.

loss functions with LFE (thin solid lines) and without LFE (thick solid lines) reproduce all the observed peaks in the experimental spectra (dotted lines). Inclusion of LFE improves the agreement between calculated and experimental spectra this is especially the case for peak positions and intensity for energy losses above 18 eV.

At energy losses below 5 eV, the calculated spectra show a small peak P* at 0.95 eV and peak A* observed at ~3 eV. On the other hand, peak A in the experimental spectra is observed at 1.37 eV. Within this energy range, spectra calculated with and without the inclusion of local field effects are very similar. The ε_{2xx} curve (thin dotted line) shown in Fig. 4(b) displays free electron behaviour at low energy falling steeply from a large positive value. Peaks in ε_2 curve are found at 8.5 eV, 16 eV, and 22 eV. The corresponding ε_{1xx} curve (thin solid line) shows free electron behavior at low energies rising from a large negative value and crosses the energy axis with a positive slope at three positions, 0.8 eV, 11.1 eV, and 28.5 eV. Interband transitions will give rise to peaks in the ε_2 curve while in metallic systems plasmon peaks obey the condition $\varepsilon_1 = 0$ with ε_2 being small.[30–33] The arrows in Fig. 4(b) mark where the ε_1 crosses the energy axis with a positive slope. We therefore expect plasmon peaks close to 0.8 eV, 11.1 eV, and 28.5 eV. This corresponds to a charge-carrier plasmon at 0.8 eV (peak P*) and two bulk plasmons at 11.1 (peak C) and 28.5 eV (peak F). The experimental peak A is therefore observed in an energy loss region between the charge carrier plasmon as well as the onset of interband transitions involving the Ni3d-O2p states at/near the Fermi level.[24,34,35] Similar peaks have been observed in several metallic transition metal oxides including ReO_3, WO_3, and Na_xWO_3 and have been described as interband plasmons attributed to hybrid resonance from interaction between charge carrier plasmons and lowest interband transitions.[31–33] In our case as we show below, surface excitations also contribute to the intensity at peak A.

To determine the effects of layer thickness on the spectra, we performed spectra calculations using the relativistic

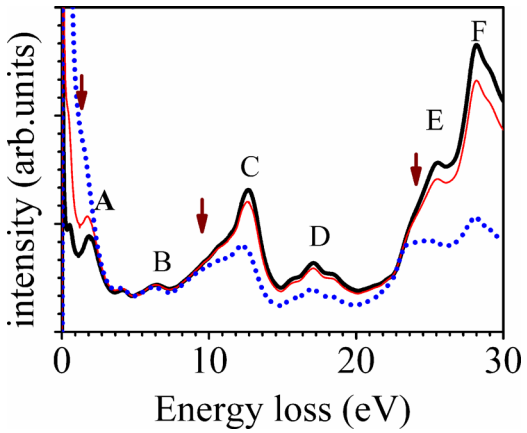

FIG. 5. Simulated EELS spectra using Kroger formalism for 100 nm (thick curve), 50 nm (thin curve), and 10 nm (dotted curve) thick $PrNiO_3$ films calculated at 80 kV. The arrows mark the changes in the spectra with decreasing sample thickness.

Kroeger formalism.[36–38] As input for these calculations, we used theoretical dielectric functions shown in Fig. 4(b). The calculated spectra for 100 nm (thick curve), 50 nm (thin curve), and 10 nm (dotted curve) thick $PrNiO_3$ films are displayed in Fig. 5. In thin 10 nm samples surface excitations contribute to the intensity at peak position A, they also give rise to a shoulder at the low energy side of the peaks C and F. Therefore, the low energy loss spectrum of a very thin $PrNiO_3$ film is dominated by surface excitations. However, their strong momentum dependence makes it possible to distinguish them from other excitations.

Finally, it is important to mention some of the challenges to this method. The first challenge involves accounting for multiple scattering effects which have been shown to increase with increasing momentum transfer.[1,8,39–41] An approach to remove multiple scattering which involves deconvolution of a momentum integrated spectrum from momentum resolved spectra has already been developed.[8] Another approach which has been proposed is to work with the MREELS spectra at low momentum transfer values ($|\boldsymbol{q}| < 1\,Å^{-1}$) since the elastic-inelastic scattering effects increase at large momentum transfer values.[39] The second issue is that low loss EELS signal is delocalized and electrons can carry information from sample regions located at a small distance L from the classical trajectory.[1] In thin films and heterostructures delocalization increases the chances of exciting surface and interface modes. As the results presented here show their strong momentum and orientation dependence (tilt) can be used to distinguish them from other transitions. Morever, the ability to obtain spatially resolved MREELS spectra means we can also investigate the dispersion behaviour of surface and interface plasmons in ultrathin layers heterostructures and nanostructures as well.

We are grateful to Eva Benckiser, Sabine Groezinger, and Willem van Mierlo for providing the TEM sample and for TEM sample preparation, respectively. We gratefully acknowledge financial support by the German Research Foundation (DFG) and the Ministry of Science, Research and the Arts (MWK) of the state Baden-Württemberg within the DFG: KA 1295/17-1 project.

[1]R. F. Egerton, Rep. Prog. Phys. **72**, 016502 (2009).
[2]J. Fink, Adv. Electron. Electron Phys. **75**, 121 (1989).
[3]K. Zeppenfeld, Z. Phys. **243**, 229 (1971).
[4]R. D. Bringans and W. Y. Liang, J. Phys. C: Solid State Phys. **14**, 1065 (1981).
[5]Y. Y. Wang, S. C. Cheng, and V. P. Dravid, Micron **30**, 379 (1999).
[6]R. B. Pettit, J. Silcox, and R. Vincent, Phys. Rev. B **11**, 3116 (1975).
[7]C. H. Chen, J. Silcox, and R. Vincent, Phys. Rev. B **12**, 64 (1975).
[8]P. E. Batson and J. Silcox, Phys. Rev. B **27**, 5224 (1983).
[9]P. Jonas and P. Schattschneider, J. Phys.: Condens. Matter **5**, 7173 (1993).
[10]G. A. Botton, J. Electron. Spectrosc. Relat. Phenom. **143**, 129 (2005).
[11]M. K. Kinyanjui, C. Kramberger, T. Pichler, J. C. Meyer, P. Wachsmuth, G. Benner, and U. Kaiser, Europhys. Lett. **97**, 57005 (2012).
[12]C. Hebert, A. Alkauskas, S. Löffler, B. Jouffrey, and P. Schattschneider, Eur. Phys. J. Appl. Phys. **54**, 33510 (2011).
[13]A. Gloter, M.-W. Chu, M. Kociak, C. H. Chen, and C. Colliex, Ultramicroscopy **109**, 1333 (2009).
[14]S. C. Liou, M.-W. Chu, R. Sankar, F.-T. Huang, G. J. Shu, F. C. Chou, and C. H. Chen, Phys. Rev. B **87**, 085126 (2013).
[15]P. A. Midgley, Ultramicroscopy **76**, 91 (1999).
[16]P. Wachsmuth, R. Hambach, M. K. Kinyanjui, M. Guzzo, G. Benner, and U. Kaiser, Phys. Rev. B **88**, 075433 (2013).
[17]H. Saito and H. Kurata, Microscopy (Tokyo) **63**, 155 (2014).
[18]F. S. Hage, Q. M. Ramasse, D. M. Kepaptsoglou, Ø. Prytz, A. E. Gunnaes, G. Helgesen, and R. Brydson, Phys. Rev. B **88**, 155408 (2013).
[19]G. Benner, H. Niebel, and G. Pavia, Cryst. Res. Technol. **46**, 580 (2011).
[20]M. A. Novojilov, O. Y. Gorbenko, I. E. Graboy, A. R. Kaul, H. W. Zandbergen, N. A. Babushkina, and L. M. Belova, Appl. Phys. Lett. **76**, 2041 (2000).
[21]M. L. Medarde, J. Phys.: Condens. Matter **9**, 1679 (1997).
[22]W. B. Wu, N. Hiraoka, D. J. Huang, S. W. Huang, K. D. Tsuei, M. van Veenendaal, J. van den Brink, Y. Sekio, and T. Kimura, Phys. Rev. B **88**, 205129 (2013).
[23]P. Blaha, K. Schwarz, G. K. H. Madsen, D. Kvasnicka, and J. Luitz, *WIEN2K: An Augmented Plane Wave and Local Orbitals Program for Calculating Crystal Properties*, edited by K. Schwarz (Vienna University of Technology, Austria, 2001).
[24]See supplementary material at http://dx.doi.org/10.1063/1.4921405 for supplementary figures and the electronic structure calculation procedure.
[25]M. Launay, F. Boucher, and P. Moreau, Phys. Rev. B **69**, 035101 (2004).
[26]P. Moreau and M.-C. Cheynet, Ultramicroscopy **94**, 293 (2003).
[27]M. K. Kinyanjui, P. Axmann, M. Wohlfahrt-Mehrens, P. Moreau, F. Boucher, and U. Kaiser, J. Phys.: Condens. Matter **22**, 275501 (2010).
[28]S. Botti, A. Schindlmayr, R. Del Sole, and L. Reining, Rep. Prog. Phys. **70**, 357 (2007).
[29]F. Aryasetiawan, O. Gunnarsson, M. Knupfer, and J. Fink, Phys. Rev. B **50**, 7311 (1994).
[30]H. Ehrenreich and H. R. Philip, Phys. Rev. **128**, 1622 (1962).
[31]J. Feinleib, W. J. Scouler, and A. Ferretti, Phys. Rev. **165**, 765 (1968).
[32]D. W. Lynch, R. Rosei, J. H. Weaver, and C. G. Olson, J. Solid State Chem. **8**, 242 (1973).
[33]R. E. Dietz, M. Campagna, and J. N. Chazalviel, Phys. Rev. B **17**, 3790 (1978).
[34]T. Arima, Y. Tokura, and J. B. Torrance, Phys. Rev. B **48**(23), 17006 (1993).
[35]M. K. Stewart, J. Liu, R. K. Smith, B. C. Chapler, C. H. Yee, K. Haule, J. Chakhalian, and D. N. Basov, J. Appl. Phys. **110**, 033514 (2011).
[36]E. Kröger, Z. Physik **216**, 115 (1968).
[37]J. P. R. Bolton and M. Chen, J. Phys.: Condens. Matter **7**, 3373 (1995).
[38]M. Couillard, A. Yurtsever, and D. A. Muller, Phys. Rev. B **77**, 085318 (2008).
[39]S. C. Cheng, Y. Y. Wang, and V. P. Dravid, Micron **27**, 167 (1996).
[40]D. S. Su and P. Schattschneider, Philos. Mag. A **65**, 1127 (1992).
[41]G. Bertoni, J. Verbeeck, and F. Brosens, Microsc. Res. Tech. **74**, 212 (2011).